J. metamorphic Geol., 2002, **20,** 351–363

The *P–T* record of synchronous magmatism, metamorphism and deformation at Petrel Cove, southern Adelaide Fold Belt

G. ALIAS,[1] M. SANDIFORD,[2] M. HAND[3] AND B. WORLEY[2]
[1]*Departament de Geoquimica, Petrologia i Prospeccio Geologica, Universitat de Barcelona, 08028 – Barcelona, Spain (gemma@natura.geo.ub.es)*
[2]*School of Earth Sciences, University of Melbourne, Victoria 3010, Australia*
[3]*Department of Geology and Geophysics, University of Adelaide, South Australia 5005, Australia*

ABSTRACT Porphyroblastic schists in the thermal aureole of the Victor Harbor Granite at Petrel Cove, in the southern Adelaide Fold Belt, South Australia, preserve a record of sequential cordierite, andalusite, staurolite, fibrolite, chlorite and muscovite growth (along with biotite + plagioclase + quartz + ilmenite) during progressive deformation. A *P–T* pseudo-section appropriate to biotite-saturated assemblages in KFMASH shows that the sequence of mineral reactions records increasing pressure of at least 1 kbar (from *c.* 3 to *c.* 4 kbar) during cooling from around 580 °C. Heating at pressures below *c.* 3 kbar is inferred for growth of early formed cordierite porphyroblasts, and is attributed in part to the thermal effects of granite emplacement, while the pressure increase is attributed to tectonic burial accruing from ongoing deformation. The 'anticlockwise' *P–T* path is consistent with convergent deformation being focussed as a consequence of heating, as to be expected for a lithospheric rheology that is strongly temperature dependent.

Key words: anticlockwise *P–T* paths; cordierite; andalusite; staurolite.

INTRODUCTION

The record of sequential porphyroblast growth and fabric development in metamorphic rocks potentially provides important insights into the interaction between deformation and heating during orogenesis. As such, metamorphic studies can contribute to our understanding of the mechanical evolution of orogenic belts. Because the mechanical response of the lithosphere is sensitive to its thermal state, we might expect that heating associated with metamorphism influences the rate and/or style of associated deformation, with this record encoded in the pressure–temperature (*P–T*) path of metamorphic rocks. For example, Sandiford *et al.* (1991) suggested that 'anticlockwise' *P–T* paths involving heating at lower pressures followed by cooling at higher pressures are a natural consequence of strain localization due to thermal weakening associated with the ascent of magma through the crust and upper mantle.

The ideas of Sandiford *et al.* (1991) were motivated by field observations in the southern Adelaide Fold Belt, where early Palaeozoic metamorphism and deformation accompanied, and were intimately associated with, the intrusion of a suite of isotopically primitive granites (e.g. Sandiford *et al.*, 1992). Rock sequences in the higher-grade parts of the southern Adelaide Fold Belt in the Mount Lofty Ranges of South Australia are dominated by psammitic schists with relatively simple, unreactive mineralogy involving mainly biotite–plagioclase–quartz–ilmenite assemblages (e.g. Offler & Fleming, 1968; Dymoke & Sandiford, 1992; Sandiford *et al.*, 1995). Consequently, there has been little detailed documentation of the thermal evolution of individual metamorphic rocks from this region. This study focuses on the *P–T* record preserved in porphyroblastic schists at Petrel Cove in the Victor Harbor region, that contain an excellent record of porphyroblast growth (cordierite, andalusite, staurolite and chlorite) in the thermal aureole of the Victor Harbor Granite. The porphyroblastic schists at Petrel Cove represent metamorphosed siltstones and are less potassic than true pelites. As a consequence, a significant part of their metamorphic evolution did not involve muscovite, and thus they cannot be understood directly in terms of KFMASH petrogenetic grids calculated for bulk compositions saturated in muscovite (e.g. Dymoke & Sandiford, 1992). In order to interpret the *P–T* evolution of the Petrel Cove sequence we describe a new *P–T* pseudosection appropriate to semipelitic schists calculated using the 1996 'tutorial' update of the thermodynamic dataset of Holland & Powell (1990).

REGIONAL GEOLOGICAL SETTING

The southern Adelaide Fold Belt records deformation, magmatism and metamorphism during the Cambrian-Ordovician Delamerian Orogeny (Sandiford *et al.*, 1992). The fold belt forms part of a large orogenic system associated with contractional deformation along

the palaeo-Pacific margin of Gondwana which further east involved accretion of volcanic arc terranes (Flottmann *et al.*, 1993).

In the southern Adelaide Fold Belt, the Delamerian Orogeny is marked by the inversion of late Proterozoic and early Cambrian extensional basins. Like many orogens, the southern Adelaide Fold Belt is characterized by distinctive external and internal domains. The external foreland, along the western and north-western margins of the belt, is characterized by low-grade metasedimentary rocks (greenschist to subgreenschist facies) with displacements mainly occurring on discrete foreland-propagating thrust surfaces (Jenkins & Sandiford, 1992; Flottmann *et al.*, 1993). The internal, eastern and south-eastern, parts of the belt are characterized by higher metamorphic grades (greenschist to amphibolite facies), abundant magmatic rocks, and more pervasive deformation styles characterized by large-scale upright fold structures.

The principal deformation phase in the internal parts of the orogen is manifest in the development of a pervasive foliation (S2), axial planar to regional-scale, upright folds (D2 of Sandiford *et al.*, 1995). A younger deformation phase that may represent the on-going D2 deformation (see later discussion) is evident in the widespread development of a crenulation cleavage broadly parallel with S2. In the highest-grade parts of the belt, an earlier phase of deformation (D1) is indicated by the development of a layer-parallel fabric folded by the upright folds (Sandiford *et al.*, 1992, 1995; Oliver & Zakowski, 1995). This fabric (S1), which is contained within a subhorizontal enveloping surface, occurs in the intrusive Rathjen Gneiss (516 ± 4 Ma), thereby providing an upper age limit to the deformation (Fig. 1, Foden *et al.*, 1999). In the Reedy Creek region in the eastern Mount Lofty Ranges (Fig. 1), granites with ages as young as 490 Ma (Sandiford *et al.*, 1995; Foden *et al.*, 1999) contain the upright fabric but not the S1 fabric, while other granites and mafic intrusives with isotopically

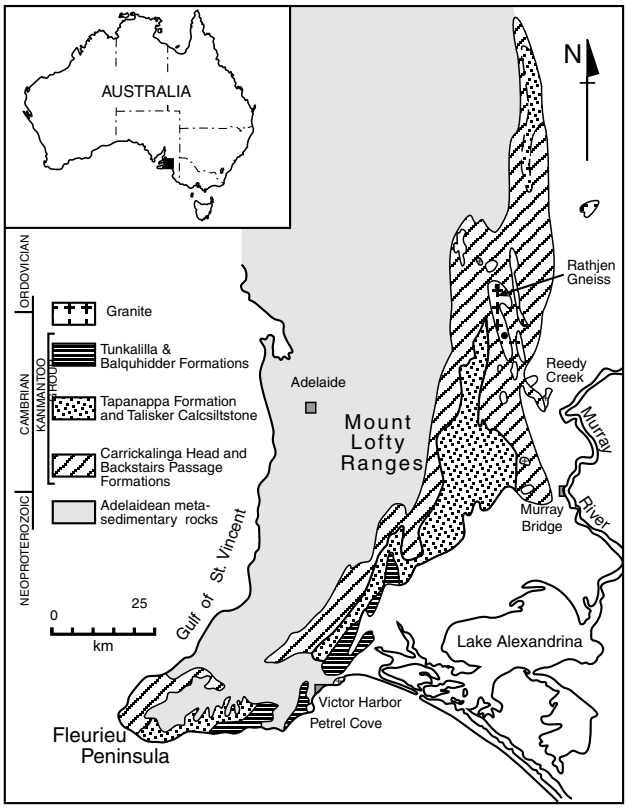

Fig. 1. Geological map of the southern Adelaide Fold Belt showing the main pre-Delamerian stratigraphic elements of the southern Adelaide Fold Belt and the location of Petrel Cove at Victor Harbor, as well as other localities mentioned in the text.

indistinguishable ages remain essentially undeformed. These observations imply that the bulk of the shortening associated with propagation of upright folds accumulated in no more than a few million years. The notion of rapid propagation of folds is further supported in the Karinya syncline in the eastern Mount Lofty Ranges where, at the largest scale, isograds are folded with about half the amplitude of the enclosing stratigraphy. Following Sleep's (1979) analysis of the rate of thermal relaxation during fold amplification, Sandiford *et al.* (1995) showed that the preserved geometry is consistent with fold amplification over a period of 0.1–1 Myr.

The simplicity of the macroscopic outcrop pattern evident in map-scale relations throughout the southern Adelaide Fold Belt (e.g. Offler & Fleming, 1968; Fig. 1) is reflected in the general absence of fold-interference patterns at the mesoscopic scale, but contrasts with the complexity evident at the microscopic scale. In particular, throughout the belt porphyroblastic schists show complex microstructures involving multiple crenulation episodes. As alluded to above, Sandiford *et al.* (1995) recognized a three-phase porphyroblast-foliation history in porphyroblastic schists from the eastern Mount Lofty Ranges. In contrast, Adshead-Bell & Bell (1999) recognized at least five phases of foliation development in the central Mount Lofty Ranges which they attributed to successive increments of strain associated with overprinting steep and shallow foliations superposed on the large-amplitude D2 folds. In contrast with the porphyroblastic schists, psammitic schists typically show only simple microstructures preserving evidence for only one episode of foliation formation axial to the D2 fold train.

Throughout the southern Adelaide Fold Belt metamorphic grade increases with proximity to syn-tectonic granites (e.g. Offler & Fleming, 1968; Dymoke & Sandiford, 1992) suggesting a close relationship that has been discussed at length by Sandiford *et al.* (1992). The isotopically primitive nature of the granites implies a mantle source component (e.g. Foden *et al.*, 1999). Consequently Sandiford *et al.* (1991) argued that the granites represent a prime crustal heating mechanism, rather than reflecting crustal melts developed as a consequence of metamorphism. As in many intermediate-temperature, low-pressure metamorphic belts there is insufficient granite in the current exposures to account for the observed distribution of metamorphic grades, if one assumes a reference frame of a normal crustal geotherm. Therefore, uncertainty remains about the extent to which the inferred metamorphic thermal regime reflects the response to: (1) prior rifting associated with the deposition of the early Cambrian Kanmantoo Group (in the interval 525–516 Ma Cooper *et al.*, 1992; Liu & Fleming, 1990; Chen & Liu, 1996; Foden *et al.* (1999) (2) elevated crustal heat production as indicated by modern day heat flows of *c.* 80 mWm^{-2} (e.g. Cull, 1982; Sandiford & Hand, 1998) or (3) additional syn-tectonic magmas emplaced above (and below) the current erosion levels.

The Victor Harbor Granite (Fig. 2) forms part of a belt of granites outcropping discontinuously as a set of headlands and islands along the south coast of Fleurieu Peninsula and Kangaroo Island. Structural relationships amongst the various granites that comprise this belt (e.g. Port Elliot Granite, Cape Willoughby Granite, the various Vivonne Bay granites, Remarkable Rocks Granite) suggests that magmatism spanned almost the entire history of deformation, consistent with observation in the eastern Mount Lofty Ranges (e.g. Sandiford *et al.*, 1992, 1995).

GEOLOGY OF PETREL COVE

Petrel Cove, on the south coast of the Fleurieu Peninsula near Victor Harbor (Fig. 1), provides an excellent coastal exposure of the contact between the Victor Harbor Granite and metasediments of the Petrel Cove Formation (Kanmantoo Group, Milnes *et al.*, 1977). The Petrel Cove Formation is composed of fine-grained metapsammites and metasiltstones, interbedded on the 0.1–1 m scale that contain abundant small-scale sedimentary structures such as load casts, cross bedding and graded bedding (Daily & Milnes, 1973). This sequence dips generally south-east, right-way up.

The Petrel Cove metasediments have been metamorphosed to porphyroblast-free, psammitic schists and porphyroblast-rich,

metasiltstones. Porphyroblast development is restricted to an aureole extending several hundred metres from the Victor Harbor Granite. The Petrel Cove sequence shows evidence for at least three phases of foliation development (Steinhardt, 1989) and a prominent metasomatic layering which we designate Sm, characterized by thin quartz septa (with accessory monazite) surrounded by thicker, pale-coloured zones that are comparatively depleted in biotite. The metasomatic nature of the layering is demonstrated by the paucity of porphyroblasts (Fig. 3), in otherwise porphyroblast-rich layers. Individual Sm microlithons are of the order of 1 cm in width. The confinement of Sm to the vicinity of the Victor Harbor Granite suggests it is associated with granite emplacement (see further discussion below), most probably representing discrete zones of enhanced permeability that have facilitated metasomatic alteration of the metasediments. The earliest recognizable phase of foliation development is preserved as inclusion trails in the earliest-formed cordierite porphyroblasts. A pervasive schistosity, S2, forms an axial planar foliation to mesoscopic, upright folds developed in the wave cut platform (Fig. 2) which, in turn, are parasitic to a regional scale anticline. The S2-fabric is defined by the preferred orientation of biotite and generally dips steeply south-east parallel to the western margin of the Victor Harbor Granite (Fig. 2). A crenulation cleavage (S3) is formed locally in the metasiltstones, typically at low angles to the S2 fabric although locally at very high angles (Fig. 3). The crenulation is expressed in both the S2 and in the earlier formed Sm layering. Interestingly, the S2 and S3 fabrics are essentially indistinguishable in metapsammitic layers even when they are clearly distinguishable in adjacent metasiltstones (Fig. 3). The distinct microstructural responses of the metapsammites and metasiltstones may simply reflect differences in the ability of the S2 foliation to track the incremental strain history. Thus, the S3 crenulations appear to have nucleated in the metasiltstones at a relatively early stage in the microstructural evolution while the S2 foliation continued to track the incremental strain history in the adjacent metasiltstones. The early 'locking' of the S2 foliation in the metasiltstones may be in part due to the heterogeneities provided by porphyroblasts.

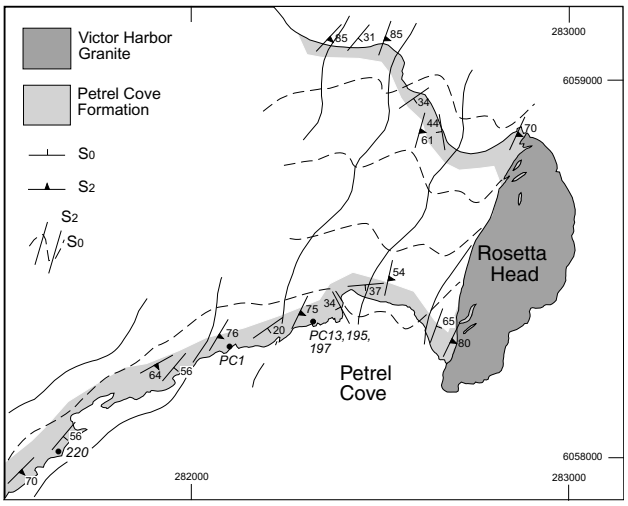

Fig. 2. Geological map of Petrel Cove showing the main geological units, the main trends of regional schistosity and bedding. Dots show locations of analysed samples.

Three chemically and structurally distinct intrusive phases are evident at Petrel Cove, namely:

1 metamorphosed dolerite dykes, typically 0.8–2 m thick, intruded prior to the development of S2.

2 boudinaged quartz–feldspar–muscovite–tourmaline pegmatites <0.3 metres thick, which intruded prior to, or early in the development of, S2 (Fig. 4a).

3 the Victor Harbor Granite, which comprises a megacrystic K-feldspar, biotite granite. Away from its intrusive contact with the surrounding metasediments, the granite is essentially unstrained. Along this contact, the granite contains numerous enclaves of metasediment, which were foliated, but not crenulated, before incorporation into the granite (Fig. 4b). Local deformation of the granite is evident however, in weak foliation development along its margin.

While the general absence of the S2 foliation in the Victor Harbor Granite at Petrel Cove implies the granite intruded late in the

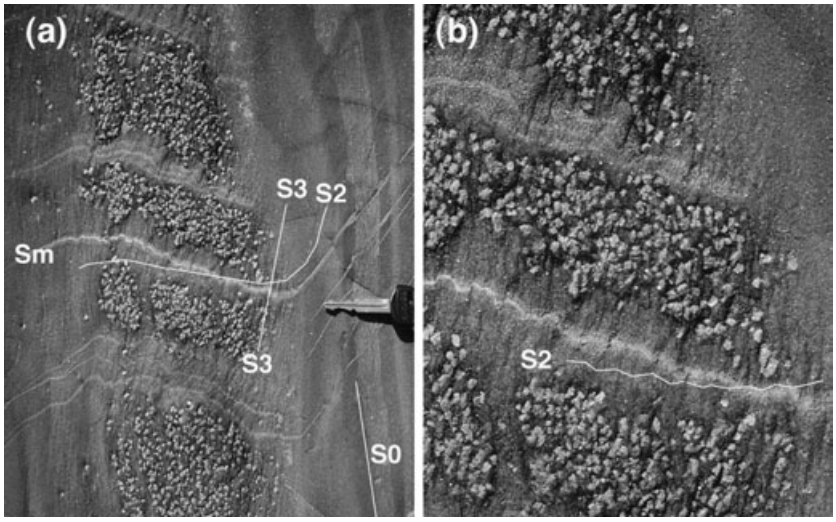

Fig. 3. Details of main structural fabrics observed at the outcrop scale. Fig. 3(b) shows a detail of Fig. 3(a). Primary compositional layering (S0) is evident by interlayering of porphyroblast-free, psammitic schists and porphyroblast-rich, metasiltstones (most porphyroblasts in this rock are andalusite). A metasomatic layering cross cuts the S0 layering. This layering originated as planar sets of shear fractures, and has been differentially rotated between porphyroblastic layers and the enclosing psammites. A crenulation cleavage (S3) evident in the porphyroblastic layers deforms an earlier formed pervasive schistosity (S2) formed at a low angle to Sm. S2 and S3 cannot be distinguished in cores of the psammitic layers. Note that the Sm layering is only crenulated in the porphyroblastic layers, implying that the psammitic layer has not been through the crenulation event. Key in (a) is 8 cm in length.

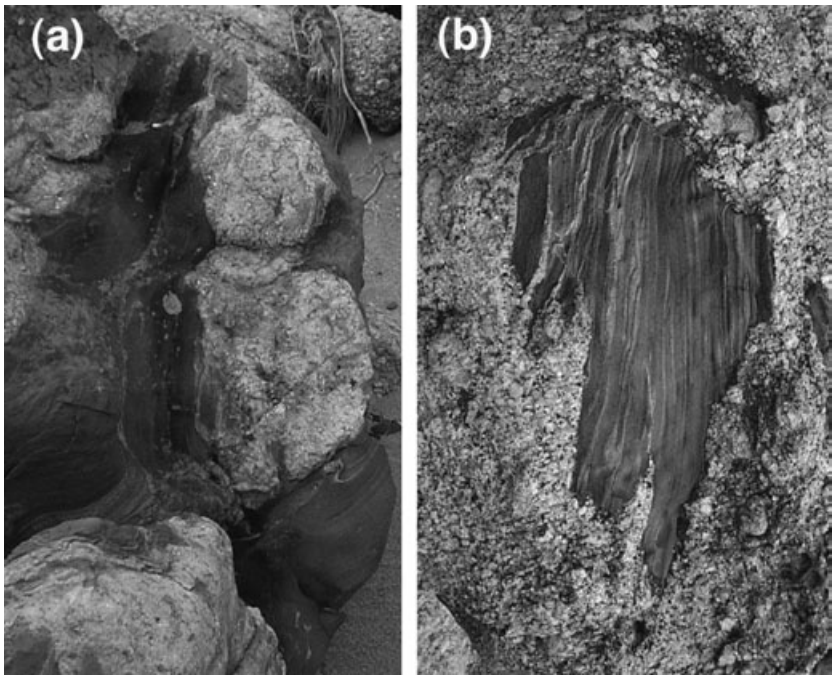

Fig. 4. (a) Boudinaged quartz–feldspar–muscovite–tourmaline pegmatites, long axes of boudins parallel the S2 fabric. Photograph width is *c.* 1 m (b) megacrystic Victor Harbor Granite including raft of foliated metasediment. The granite is only weakly deformed and its intrusion clearly exploits the S2 foliation in metasediments, implying emplacement late in the deformation history.

deformation history, magmatic activity earlier in the deformation history is suggested by (1) the restricted development of the metamorphic assemblages described here, which are indicative of locally elevated temperatures during S2, and somewhat more circumstantially by (2) the restriction of the Sm layering developed prior to S2, to the immediate neighbourhood of the granite. Early formed pegmatite dykes, now boudinaged within S2, support the notion that deformation and metamorphism was intricately linked with magmatism throughout the orogenic cycle, as observed elsewhere within the southern Adelaide Fold Belt (e.g. Sandiford *et al.*, 1992, 1995). Available geochronological data (Dasch *et al.*, 1971; Milnes *et al.*, 1977) suggest an age of 508 ± 14 Ma (Rb/Sr $\lambda = 1.42 \times 10^{-11}$ yr^{-1}, Liu & Fleming, 1990) for the Encounter Bay Granite.

Metasomatic alteration is evident in a number of discrete, pale-coloured, steep dipping zones up to 1 m wide. The bleached appearance of these zones reflects depletion in biotite and contrasts markedly with the typically dark colour of the surrounding, unaltered metasediments. Whereas these zones parallel the regional strike, they are locally discordant to S0. One such zone along the intrusive contact of the granite clearly alters the granite and therefore must postdate its emplacement. Dasch *et al.* (1971) showed that this zone has the same Sr-isotopic composition as the granite and concluded that metasomatism occurred in response to infiltration of fluids derived from the granite.

PETROLOGY

Metasiltstones from the Petrel Cove Formation contain several mineral associations that preserve a record of sequential porphyroblast growth. The main assemblages (Table 1) always involve biotite + quartz + plagioclase + ilmenite with minor tourmaline, zircon, apatite and rutile. In addition to these matrix-forming minerals, the metasiltstones typically contain one or more of the following: cordierite, andalusite, staurolite, chlorite and muscovite. In many cases, the main porphyroblast may form nearly 50 modal percent of the rock. In addition, sillimanite occurs as fibrolitic needles in a number of samples. The Petrel Cove metasiltstones represent a compositional spectrum between two end-members represented by:

- more magnesian, cordierite-rich assemblages (e.g. PC1, Table 1, Fig. 5), and
- less magnesian, andalusite-rich, cordierite-absent assemblages (e.g. 195C, Table 1).

Samples with intermediate composition (e.g. samples PC13 & 220, Table 1) contain significant modal proportions of both cordierite and andalusite. Below we provide a brief summary of the textural observations pertinent to the relative timing of growth of each of the main phases.

Table 1. Main mineral assemblages from Petrel Cove Formation metasiltstones.

	Modal proportions									
Mineral assemblages	mtx/pb	and	crd	sil	st	bt	chl	ms	qtz	Samples
qtz-bt-crd-and ± chl ± ms	80/20	2	18	–	–	39	<1	1	39	PC1
qtz-bt-crd-and/sil-st ± chl ± ms	60/40	25	15	1	1	25	4	2	17	PC13
	60/40	35	5	0.5	0.5	27	2	2	28	195C
	80/20	10	10	2	2	31	7	4	34	220
qtz-bi-crd-and-ms ± chl ± ms	85/15	12	3	–	–	30	5	10	40	195B

Textural characteristics of the main phases

The matrix-forming minerals range in size from 0.1 to 0.3 mm, although biotite crystals can reach 0.8 mm in length. Biotite, ilmenite and quartz occur as S1-defining inclusion traces in cordierite (see below), form the main component of S2 and form polygonal mosaics in S3 crenulations. These observations imply that they were stable through all recognized deformation events.

Cordierite forms equant to elongate, rounded poikiloblasts, 1–4 mm in length. Inclusions of quartz,

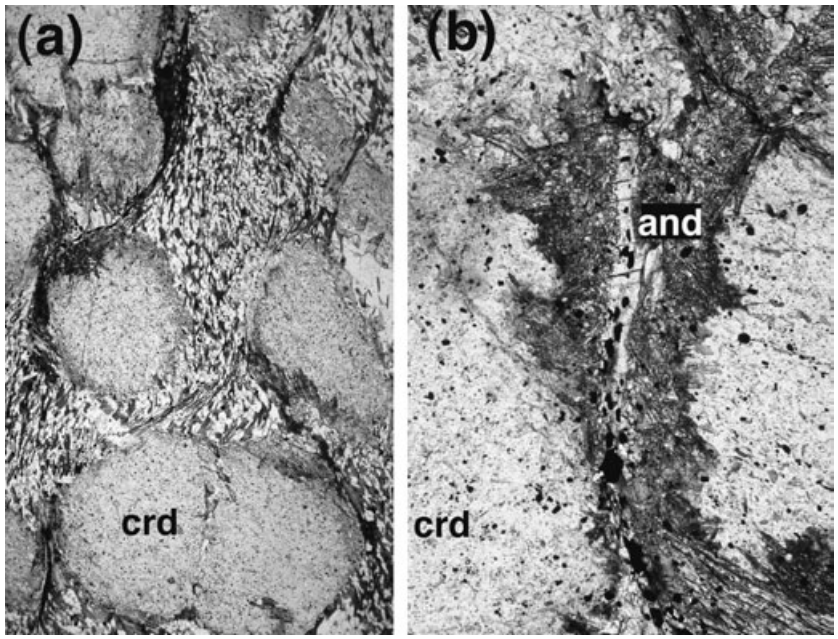

Fig. 5. Characteristic microstructure in relatively magnesian, cordierite-rich bulk compositions (Sample 95/5). The wrapping of S2 about cordierite porphyroblasts implies growth early in the development of S2 (a). Adjacent cordierite porphyroblasts are characteristically separated by planar rims of poikiloblastic andalusite (b). In the matrix immediately neighbouring andalusite, chlorite is characteristically developed and partly contained within the S2 fabric and partly overgrowing it, suggesting relatively late formation of andalusite + chlorite in S2 (see Fig. 16a). Compared to the surrounding matrix, the core regions of the andalusite-bearing domains commonly contain more ilmenite, implying ilmenite growth accompanied initial andalusite formation involved Ti-Tschermaks exchange with biotite. Width of field is *c.* 10 mm in (a) and *c.* 1.5 mm in (b).

ilmenite and biotite define straight to gently curved trails at a high angle to the external S2 foliation. The internal foliation may be continuous or discontinuous with the external S2 fabric and is interpreted to reflect an older foliation (S1). Where it is continuous with S2, the outer portion of the cordierite contains a smoothly curving foliation that links the inclusions in the interior of the porphyroblast with the matrix. The gently curved trace of the inclusion trails together with its frequent discordance with S2 suggests that cordierite began to grow early during the shortening associated with S2 (Fig. 6). Where S3 is developed, cordierite shows evidence of microboudinage (see also Steinhardt, 1989). Cordierite has not been observed to include pre-existing porphyroblastic phases implying that it is the first formed porphyroblast.

Andalusite occurs in several textural forms depending on the bulk composition of the rock. In the Mg-rich bulk compositions it forms overgrowths on cordierite (Fig. 5). These overgrowths are best developed as thin seams parallel to S2 where adjacent cordierite porphyroblasts meet. In less magnesian compositions, andalusite is more abundant, but also clearly overgrows cordierite (Fig. 6). In these instances, the inclusion trails in the andalusite are generally continuous with those in the cordierite. However the included quartz in the andalusite is noticeably more elongate than in the cordierite, suggesting some foliation development occurred between the cordierite and andalusite growth. Even where the inclusion trails in the interior of the andalusite are at a high angle to the external S2 they invariably curve continuously into it (Fig. 6). In some instances poikiloblastic andalusite is mantled by delicate symplectitic aggregates of andalusite, which appears to overgrow S2 fabrics (Fig. 7). In

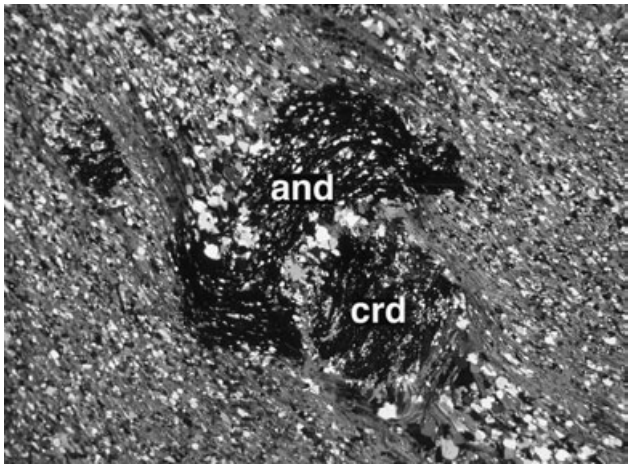

Fig. 6. Composite porphyroblast with andalusite overgrowing cordierite, in an intermediate bulk composition. Both the andalusite and cordierite contain an early foliation (S1) progressively overgrown by the blasts during the early stages of S2 crenulation (see Fig. 16b). Width of field is *c.* 5 mm.

rocks with low modal cordierite ($< c.$ 10%), inclusion trails in andalusite show relatively minor deflections into S2, suggesting it grew somewhat later than in the more Mg-rich bulk compositions. In the most Fe-rich assemblages with little or no cordierite, andalusite forms xenoblastic to subidioblastic poikiloblasts up about 5–6 mm in diameter in the microlithon domains of S3 crenulations (Fig. 8) locally preserving millipede structures confirming its syn-kinematic growth during progressive S3 crenulation of S2.

Sillimanite occurs in a number of sections in trace amounts as fibrolitic needles developed close to andalusite along with staurolite, chlorite (Fig. 9) or

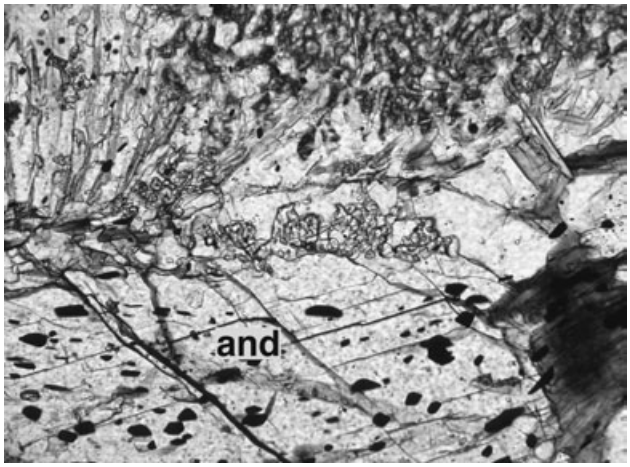

Fig. 7. Andalusite porphyroblast mantled by a later generation of finer grained andalusite (Sample 95/4). Width of field is *c.* 0.5 mm.

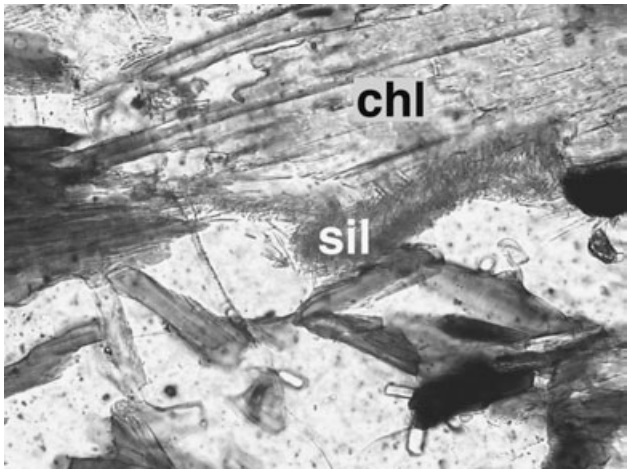

Fig. 9. Fine-grained fibrolite partly mantles S2 parallel chlorite (sample 95/5). Width of field is *c.* 0.4 mm.

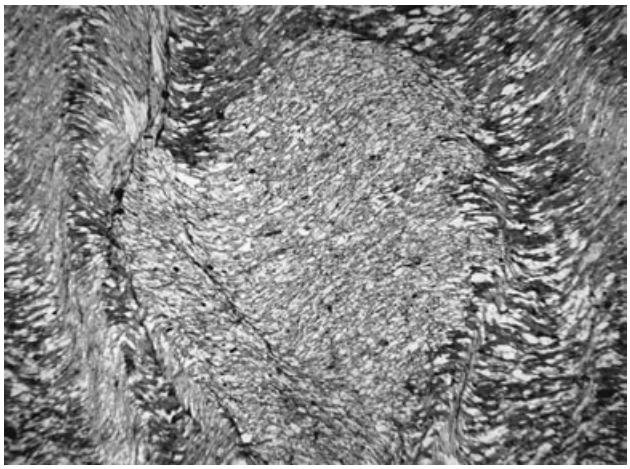

Fig. 8. Large andalusite poikiloblast showing development of S3 crenulations. This cordierite-free assemblage contains muscovite in the matrix (sample 95/6). Width of field is *c.* 3 mm.

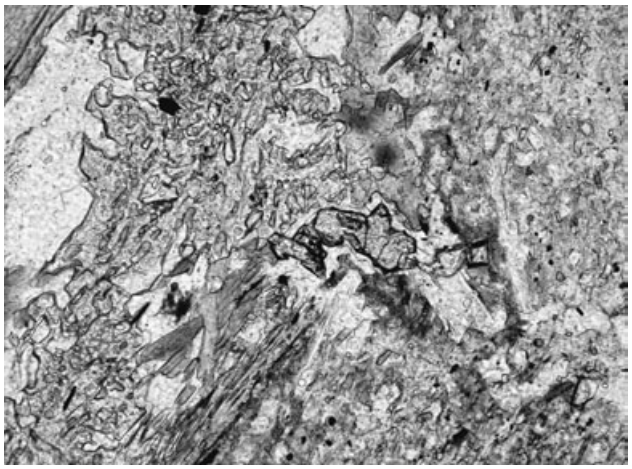

Fig. 10. Idioblastic staurolite associated with andalusite and chlorite that have partly replaced cordierite, note that chlorite overgrows S2 foliation (sample 95/5). Width of field is *c.* 0.4 mm.

muscovite. Locally, it also parallels S2, and is included in quartz in pressure shadows around andalusite, suggesting that it grew during the deformation. Staurolite forms small crystals up to 0.1 mm in length with modal amounts typically <1–2%, mostly intergrown with andalusite (Fig. 10) and/or muscovite and chlorite (Fig. 11) as overgrowths on cordierite. In rare instances, it is included in the outer parts of andalusite poikiloblasts. In some places, staurolite is intergrown with fibrolite. Chlorite typically occurs as euhedral blasts cutting both S2 and S3. As an epitaxial replacement of biotite, it takes a mimetic form parallel to S2. It also forms decussate aggregates rimming the embayed faces of cordierite. In other instances, it occurs together with staurolite and muscovite in the pressure shadows of microboudinaged cordierite porphyroblasts developed during S3 crenulation. Muscovite mostly occurs as postkinematic blasts up to 2 mm in length that crosscut both S2 and S3.

In summary, the textural features of the Petrel Cove porphyroblastic schists described above suggest that the temporal sequence of mineral growth involved firstly cordierite, followed by andalusite and, lastly, sillimanite and staurolite growth coeval with chlorite and muscovite (Fig. 12). The growth of andalusite appears to be progressively delayed with increasing bulk-rock Fe-content.

Inferred reaction sequence

In this section, we focus the reaction history in metasiltstones of intermediate composition (e.g. PC1, Fig. 6), that typically comprise significant modal proportions of both cordierite and andalusite. As

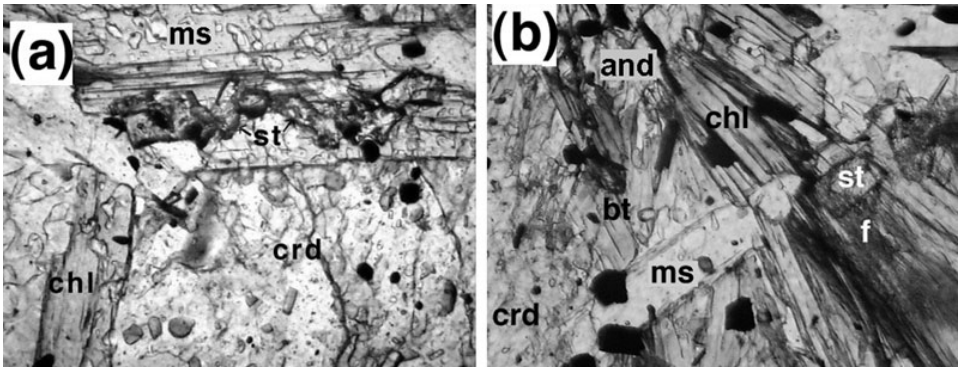

Fig. 11. (a) Intergrowth of staurolite, muscovite and chlorite in cordierite–biotite schist (sample 95/5). (b) Intergrowth of chlorite, biotite, muscovite, staurolite, fibrolite and andalusite between earlier formed cordierite blasts (sample 95/5). Width of field is *c.* 0.5 mm in (a) and *c.* 0.3 mm in (b).

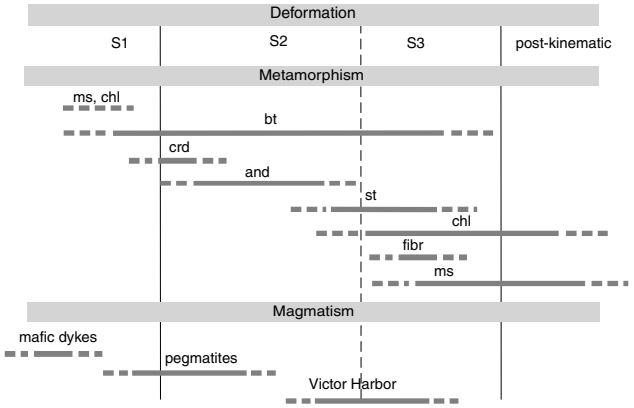

Fig. 12. Schematic relationship of chronology of mineral growth in intermediate metasiltstones that typically contain around 15 modal percentage cordierite and 5 modal percentage andalusite in the Petrel Cove Formation. In more Fe-rich compositions, andalusite growth occurs later in the history.

summarized above the textures in these rocks suggest the progressive growth of cordierite, followed by andalusite and, finally, staurolite, chlorite, sillimanite and muscovite.

In the absence of remnants of precordierite ferromagnesian-phase assemblage, it seems most probable that cordierite growth during the prograde metamorphic cycle occurred in response to chlorite breakdown:

$$\mathrm{chl} + \mathrm{ms} \rightarrow \mathrm{crd} + \mathrm{bt} \qquad (1)$$

and the related Tschermaks exchange reactions as outlined by Pattison (1987). While this stage of the reaction history was probably limited by chlorite modes, it would also have served to deplete rocks in muscovite, leaving the characteristic earliest recognized (syn-S2) association of cordierite–biotite–quartz.

A reaction enabling the formation of andalusite is the KFMASH divariant reaction involving the replacement of cordierite + muscovite. Generally andalusite surrounds cordierite and locally includes it:

$$\mathrm{crd} + \mathrm{ms} \rightarrow \mathrm{and} + \mathrm{bt} \qquad (2)$$

The reaction would account for the spatial association between andalusite and cordierite. The availability of muscovite may well have provided the critical factor in dictating which rocks developed andalusite, with this reaction serving to further deplete muscovite. An alternative possibility is that andalusite growth occurred via a Tschermaks exchange ($Al_2(MgFe)_{-1}Si_{-1}$) involving biotite and quartz (e.g. Pattison, 1987):

$$\mathrm{crd} + \mathrm{tsch} + \mathrm{qtz} \rightarrow \mathrm{and} \qquad (3)$$

A variant of this reaction involving Ti-Tschermaks molecule in biotite ($TiAl_2(MgFe)_{-1}Si_{-2}$) is suggested by the common association of andalusite and ilmenite in reaction textures replacing cordierite (Fig. 6b):

$$\mathrm{crd} + \mathrm{Ti\text{-}tsch} + \mathrm{qtz} \rightarrow \mathrm{ilm} + \mathrm{and} \qquad (4)$$

The amount of andalusite that could grow via reactions involving Tschermaks exchanges in biotite is relatively small, and thus cannot explain all andalusite in the cordierite-bearing assemblages. Near cordierite, andalusite is commonly associated with chlorite suggesting the FMASH divariant contributed to its growth:

$$\mathrm{crd} \rightarrow \mathrm{and} + \mathrm{chl} \qquad (5)$$

This reaction has the potential to produce a larger modal proportion of andalusite than the reaction involving the Tschermaks exchange and, in principle, could lead to the loss of cordierite from the assemblage. However, the textures suggest that chlorite growth postdates the great majority of andalusite growth. Therefore, this reaction could only be responsible for the last stages of andalusite growth.

A possible reaction for the production of staurolite is the FMASH divariant involving the breakdown of cordierite and andalusite:

$$\mathrm{and} + \mathrm{crd} \rightarrow \mathrm{st} \qquad (6)$$

It is noted that the modal proportion of staurolite is very low ($\ll 1$ vol%) and it typically contains *c.* 1 wt% ZnO, suggesting that it is partly stabilised by non-KFMASH equilibria (see next section). The common intergrowth of staurolite with both chlorite and muscovite (Fig. 11) suggests that it formed in part through

the KFMASH univariant:

$$\text{crd} + \text{bt} \rightarrow \text{st} + \text{chl} + \text{ms} \quad (7)$$

We remain uncertain of the significance of sillimanite which only forms as fibrolitic needles relatively late in the reaction sequence. Its intergrowth with chlorite and staurolite (e.g. Fig. 11b) would seem to preclude its formation by the polymorphic transition of earlier-formed andalusite. As noted below, we consider that the appearance of staurolite late in the reaction history is indicative of a pressure increase, and allows that the *P–T* path entered the sillimanite stability field at this stage (see discussion below).

MINERAL CHEMISTRY

Representative electron microprobe analyses of the main ferro-magnesian phases are listed in Tables 2–6. Analyses were performed on a Cameca SX51 Microprobe located in the Centre for Electron Microscopy and Microstructure Analysis at the University of Adelaide. Matrix-forming biotite typically has X_{Fe} *c.* 0.4–0.5 and Al_{VI} *c.* 0.43–0.49 (Table 2). The most magnesian biotite is found in cordierite-rich assemblages (PC1, $X_{Fe} = 0.43$) whereas the least magnesian biotite occurs in the andalusite-rich assemblages (195C, $X_{Fe} = 0.49$). Cordierite in the metasiltstones has $X_{Fe} = 0.3–0.35$ (Table 3), with an inverse correlation between cordierite modes and X_{Fe} (Tables 1 & 3). Chlorite has $X_{Fe} = 0.41–0.46$ and $Al_{VI} = 2.71–3.12$ (Table 5). The X_{Fe} of analysed staurolite is *c.* 0.82, and X_{Zn} is typically 0.06 (Table 6). The paragonitic content in muscovite is Ms_{pa} 0.13–0.17 and Al_{VI} *c.* 4.82–4.88 (Table 6).

Table 2. Biotite analyses from Petrel Cove Formation metasiltstones.

Ox	PC1	PC13	195B	195C	197	220
SiO_2	36.44	35.87	35.79	36.13	35.55	35.87
TiO_2	1.49	1.47	1.52	1.37	1.34	1.32
Al_2O_3	19.37	19.65	19.47	19.85	20.06	19.18
Cr_2O_3	0.07	0.04	0.01	0.04	0.12	0.00
MgO	12.23	11.27	11.02	11.00	10.89	11.54
MnO	0.19	0.18	0.30	0.18	0.16	0.12
FeO	16.48	18.64	18.62	18.59	18.91	18.84
Na_2O	0.24	0.26	0.24	0.25	0.35	0.19
K_2O	9.31	8.91	9.07	8.78	8.87	9.06
Total	95.82	96.28	96.06	96.19	96.26	96.11
Si	5.92	5.85	5.86	5.88	5.80	5.87
Ti	0.18	0.18	0.19	0.17	0.17	0.16
Al	3.71	3.77	3.76	3.81	3.86	3.70
Cr	0.01	0.01	0.00	0.01	0.02	0.00
Mg	2.96	2.74	2.69	2.67	2.65	2.82
Mn	0.03	0.03	0.04	0.03	0.02	0.02
Fe	2.24	2.54	2.55	2.53	2.58	2.58
Na	0.08	0.08	0.08	0.08	0.11	0.06
K	1.93	1.85	1.90	1.82	1.85	1.89
Total	17.04	17.04	17.06	16.99	17.06	17.09
X_{Fe}	0.43	0.48	0.49	0.49	0.49	0.48
Al^{vi}	1.62	1.62	1.62	1.69	1.66	1.57

Table 3. Cordierite analyses from Petrel Cove Formation metasiltstones.

Ox	PC1	PC13	197	220
SiO_2	48.53	48.05	47.77	48.14
Al_2O_3	32.47	32.56	32.65	32.27
MgO	9.39	8.43	8.69	8.75
MnO	0.35	0.62	0.60	0.38
FeO	7.13	8.09	8.20	8.13
Na_2O	0.19	0.34	0.20	0.29
Total	98.07	98.10	98.11	97.97
Si	4.99	4.97	4.94	4.96
Al	3.94	3.97	3.98	3.94
Mg	1.44	1.30	1.34	1.35
Mn	0.03	0.06	0.05	0.03
Fe	0.61	0.70	0.71	0.70
Na	0.04	0.07	0.04	0.06
Total	11.05	11.07	11.07	11.07
X_{Fe}	0.30	0.35	0.35	0.34

Table 4. Muscovite analyses from Petrel Cove Formation metasiltstones.

Ox	PC1	195C	220
SiO_2	46.47	45.93	46.24
TiO_2	0.29	0.26	0.09
Al_2O_3	36.69	36.36	35.73
MgO	0.59	0.50	0.76
FeO	0.76	0.95	1.20
Na_2O	1.23	1.27	1.36
K_2O	9.57	9.49	9.51
Total	95.62	94.92	94.92
Si	6.68	6.66	6.71
Ti	0.03	0.03	0.01
Al	6.21	6.21	6.11
Mg	0.13	0.11	0.16
Fe	0.09	0.12	0.15
Na	0.34	0.36	0.38
K	1.75	1.76	1.76
Total	15.23	15.26	15.29
Al^{vi}	4.89	4.88	4.83

Table 5. Chlorite analyses from Petrel Cove Formation metasiltstones.

Ox	PC1	PC13	195B	195C	197	220
SiO_2	27.10	24.32	24.55	24.73	24.61	25.39
TiO_2	0.29	0.09	0.08	0.11	0.11	0.11
Al_2O_3	23.07	23.32	23.05	22.73	23.25	22.98
MgO	15.68	16.19	16.49	15.96	16.18	17.75
CaO	0.09	0.05	0.04	0.01	0.01	0.02
MnO	0.29	0.42	0.48	0.49	0.36	0.24
FeO	19.91	24.63	23.96	23.52	24.43	22.34
K_2O	1.11	0.00	0.02	0.02	0.01	0.00
Total	87.54	89.01	88.67	87.56	88.95	88.83
Si	5.55	5.03	5.09	5.17	5.09	5.19
Ti	0.04	0.01	0.01	0.02	0.02	0.02
Al	5.57	5.69	5.63	5.60	5.67	5.53
Mg	4.79	5.00	5.09	4.98	4.99	5.41
Ca	0.02	0.01	0.01	0.00	0.00	0.01
Mn	0.05	0.07	0.08	0.09	0.06	0.04
Fe	3.41	4.26	4.15	4.11	4.23	3.82
K	0.29	0.00	0.01	0.01	0.00	0.00
Total	19.74	20.08	20.07	19.97	20.06	20.01
X_{Fe}	0.42	0.46	0.45	0.45	0.46	0.41
Al^{vi}	3.13	2.72	2.72	2.77	2.76	2.72

KFMASH PHASE EQUILIBRIA

The sequence of porphyroblast growth and the reactions that contributed to this sequence potentially provide important constraints on the *P–T* evolution of the Petrel Cove sequence. To elucidate this record we have used THERMOCALC v2.5 (Powell & Holland, 1988) with the 1996 'tutorial' update to the Holland and Powell dataset (Holland & Powell, 1990) to construct pseudosections appropriate to the Petrel Cove metasiltstones. Plagioclase and ilmenite do not appear to play a significant role in the preserved reaction history, and therefore, ignoring these phases the compositional variation within the Petrel Cove metasiltstones can be described by the model system KFMASH (K_2O–FeO–MgO–Al_2O_3–SiO_2–H_2O).

In comparison to most rocks which are modelled using the KFMASH system, those at Petrel Cove are not sufficiently potassic to stabilise muscovite across the full reaction history, and thus their evolution cannot be understood in terms of the normal 'pelite' KFMASH equilibria or the AFM + muscovite + quartz + H_2O compatibility diagram (e.g. Thompson, 1957; Spear & Cheney, 1989; Powell & Holland, 1990; Dymoke & Sandiford, 1992; Xu *et al*., 1994; Powell *et al*., 1998; and many others). In this paper, we have extended the standard KFMASH petrogenetic grid to include muscovite-absent [ms] equilibria (Figs 13 & 14). As biotite and quartz are ubiquitous in the Petrel Cove rocks, these have been used as saturating phases in producing a compatibility diagram which in appearance is very similar to the classic AFM diagram, but involves projection from biotite rather than muscovite (Fig. 13). It is important to note that while [ms] equilibria may well involve biotite in the equilibrium assemblage, the modal proportion of biotite is unaffected by [ms] univariant reactions, as it is the sole K_2O-bearing phase. However, in [ms] univariants, biotite does experience compositional changes via Fe–Mg and Tschermaks exchanges, and as such the composition of biotite can still be calculated in the same way as for the other phases.

In addition to biotite, quartz and H_2O, which were assumed to be in excess, the following KFMASH phases were considered in all calculations, cordierite, staurolite, chlorite, muscovite, chloritoid, garnet and the aluminosilicate polymorphs, andalusite, sillimanite and kyanite (Fig. 15). The assumption of excess H_2O implies H_2O addition during the retrograde history. The bulk composition which we have chosen to model the Petrel Cove metasiltstones is based on the sample 220 (see Table 1) with modes for cordierite (*c*. 10%) and andalusite (*c*. 10%). For this composition we have $Al_2O_3 = 35.45$, MgO = 31.49, FeO = 25.76 and $K_2O = 7.30$ referred as percentage moles.

Table 6. Staurolite analyses from Petrel Cove Formation metasiltstones.

Ox	195C	197	220
SiO_2	27.04	27.47	27.47
TiO_2	0.51	0.36	0.54
Al_2O_3	52.91	53.48	53.30
Cr_2O_3	0.14	0.04	0.17
MgO	1.66	1.66	1.72
MnO	0.75	0.57	0.49
FeO	13.23	13.45	13.80
ZnO	1.29	1.45	1.12
Total	97.53	98.47	98.62
Si	3.80	3.82	3.82
Ti	0.05	0.04	0.06
Al	8.76	8.76	8.72
Cr	0.02	0.00	0.02
Mg	0.35	0.34	0.36
Mn	0.09	0.07	0.06
Fe	1.56	1.56	1.60
ZnO	0.13	0.15	0.12
Total	14.76	14.75	14.75
X_{Fe}	0.82	0.82	0.82

The cordierite, staurolite, muscovite, biotite, quartz association at Petrel Cove

As discussed above, a number of rocks from Petrel Cove contain cordierite, staurolite, andalusite, muscovite, biotite, chlorite and quartz in close association. The association of cordierite, staurolite, biotite and muscovite is unusual, with the potential stability of this association being the subject of contention (e.g. Pattison *et al*., 1999). In the Petrel Cove rocks this association clearly occurs, but only in disequilibrium

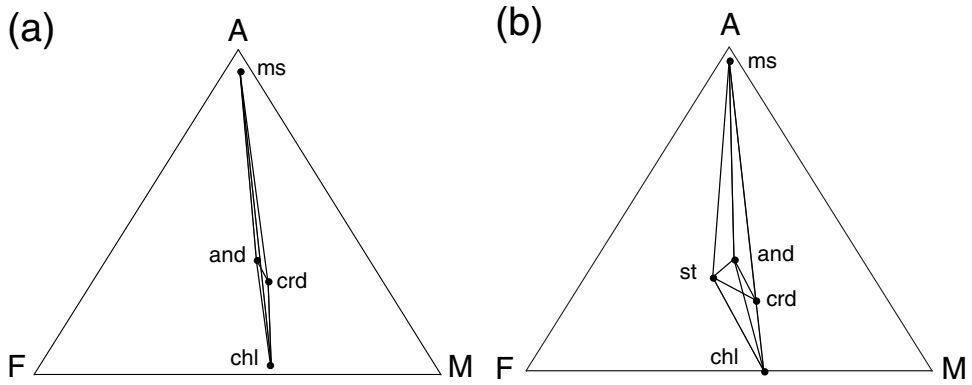

Fig. 13. AFM plotting diagrams for (a) cordierite–andalusite bearing schist and (b) cordierite–andalusite–staurolite bearing schist; quartz, biotite and water are in excess. Note that the narrow FM field in both assemblages restricts the global bulk X_{Fe} composition of the rock to 0.40 in (a) and between 0.45 and 0.50 in (b).

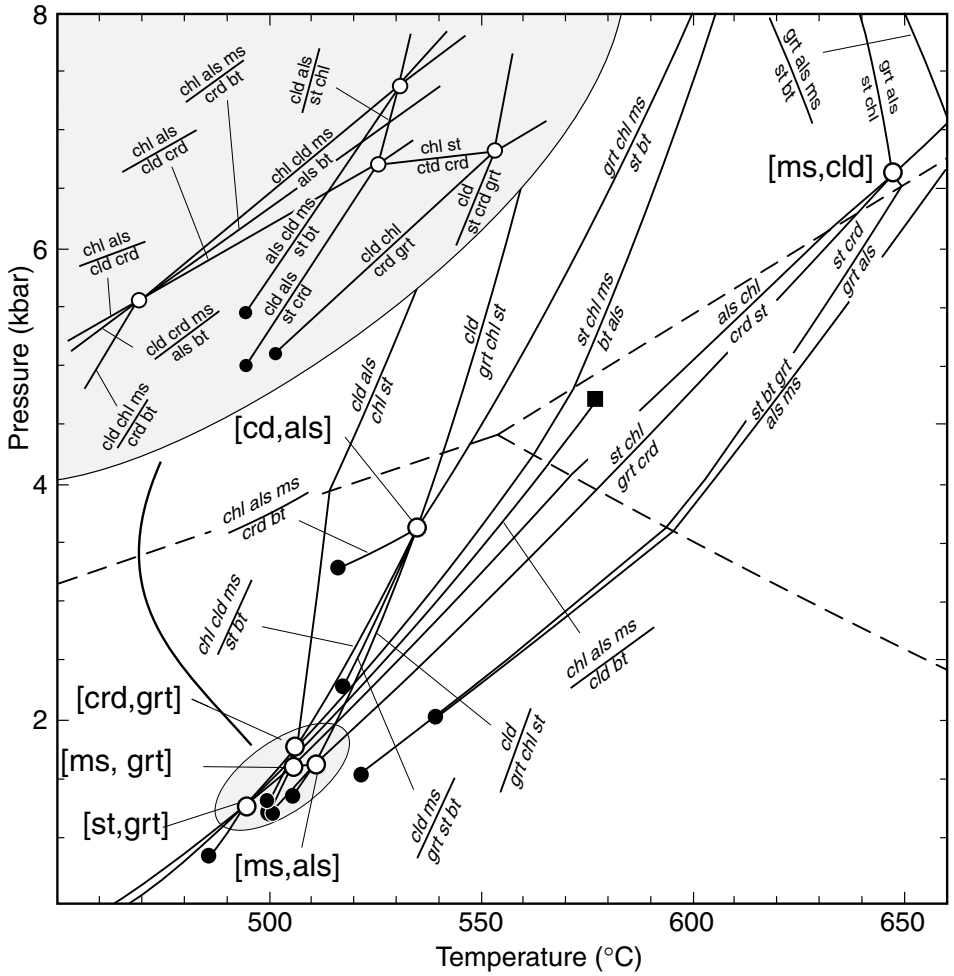

Fig. 14. Calculated *P–T* grid for the systems KFMASH and KFASH, with biotite, quartz and H_2O in excess.

assemblages indicative of the breakdown of cordierite, with staurolite formed late in the reaction history. This is unlike all other documented occurrences of this association in which early formed staurolite has been replaced by cordierite (see Pattison *et al.*, 1999). In keeping with the conclusions of Pattison *et al.* (1999), the pseudosection shown in Fig. 15 does not allow for the stable association of cordierite, staurolite, muscovite and biotite. Moreover, this pseudosection suggests that such an association will only develop along *P–T* paths that show significant changes in pressures. As argued by Pattison *et al.* (1999), this provides an appealing explanation for the fact that the association has not been documented from classic thermal aureoles where the metamorphic cycle is typically one of isobaric heating and cooling.

P–T EVOLUTION OF THE PETREL COVE FORMATION

According to the sequential crystallization interpreted from petrological observations and the assistance of the calculated pseudosection, the porphyroblastic schists from Petrel Cove followed an 'anticlockwise' *P–T* path (Fig. 15). The initial path is interpreted to involve near-isobaric heating, from *c.* 520 to *c.* 565 °C which produced cordierite in response to chlorite breakdown. This heating phase occurred either just before, or early in, the development of the S2 foliation as indicated by the presence of curved and gently crenulated inclusions within cordierite. There are no precise constraints on the slope of the prograde trajectory, or the maximum temperature reached within the cordierite–biotite–quartz field. The growth of andalusite after cordierite implies that the prograde path occurred at pressures $<c.$ 3 kbar. The retrograde path marked by the initial growth of andalusite mainly during S2 development is inferred to have involved a pressure increase of approximately 1 kbar during cooling. Although the *P–T* path through the andalusite–cordierite–biotite–quartz involves a pressure increase of *c.* 0.8 kbar, this is unlikely to have resulted in all andalusite growth since modal changes in this trivariant field are related to reactions involving Tschermaks exchange in biotite (see earlier discussion). Much of the andalusite growth

probably occurred during crossing of the narrow andalusite–cordierite–biotite–chlorite divariant, at pressures slightly lower than 4 kbar. In less magnesian, more andalusite-rich rocks, it is probable that the phase assemblage never entered the quadrivariant cordierite + biotite field on the prograde path. Rather the peak temperatures are more likely to have been attained while muscovite was still stable, and subsequent increase in pressure resulted in andalusite growth via the muscovite consuming divariant (Fig. 16) relatively early in the deformation history.

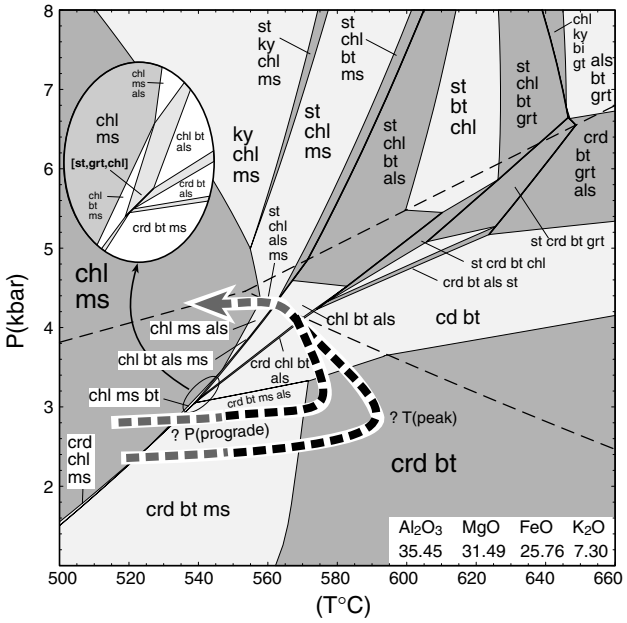

Fig. 15. Calculated *P–T* pseudosection for an aluminosilicate–cordierite–staurolite-bearing schist, showing the sequential crystallization interpreted at Petrel Cove. The black portion of the *P–T* paths corresponds to the development of S2 and S3. The average semipelite composition is expressed in mole percentage and refers to a bulk composition that contains 15 modal percentage cordierite and 5 modal percentage andalusite (see text for discussion). The two *P–T* paths bracket the range of allowable evolution on the basis of our understanding of the sequence of textures within the Petrel Cove metasiltstones.

The pseudosection in Fig. 15 suggests that in order for rocks formerly comprising only cordierite + biotite to pass through the andalusite–cordierite–biotite–chlorite divariant field within andalusite stability, there must be some cooling accompanying compression. The amount of cooling could be as little as *c.* 10 °C, although greater cooling would be implied if peak temperatures were much greater than *c.* 570 °C. The petrological relationships indicate that staurolite also grew at this time, or shortly thereafter, implying that the retrograde evolution passed through staurolite-bearing fields. However, as noted above staurolite contains appreciable ZnO (=1 wt%). The effect of ZnO will be to expand KFMASH staurolite-bearing equilibria to lower pressures and a larger temperature range than shown in Fig. 15, and to increase their variance. As a consequence of this, the *P–T* path shown in Fig. 15 is interpreted to track at pressures below those required to stabilise staurolite in the pure KFMASH system. The relatively late-stage growth of minor amounts of fibrolite is consistent with the retrograde path making a small excursion across the andalusite–sillimanite boundary (although as noted above we remain uncertain as to the *P–T* significance of fibrolite). Near-isobaric cooling, or even cooling with some decompression is implied by the growth of muscovite after fibrolite, and the absence of further staurolite or any kyanite growth at this stage of the textural evolution. The post-S3 growth of muscovite and chlorite is consistent with continued retrograde cooling but does not constrain the associated pressure changes following the last increments of deformation.

The inferred increase in temperature from *c.* 520 to *c.* 560 °C early in the development of S2 (Fig. 15) is most readily attributed to magmatic heating. While the

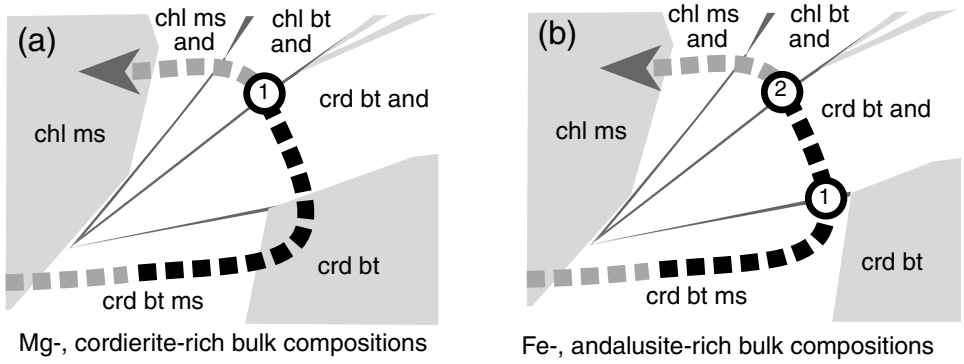

Fig. 16. Schematic *P–T* pseudosections contrasting the sequence of reactions and timing of most rapid phase of andalusite growth (circles) in (1) relatively magnesian, bulk compositions, and (b) less magnesian bulk compositions. Quadrivariant fields are shown in light grey, trivariant fields are white and divariant fields are shaded in dark greys. Note the main divariant reactions responsible for the most rapid changes in the modal proportion of andalusite occur at very different stages in the *P–T* path. In relatively Fe-rich rocks, an early phase of rapid andalusite growth is to be expected (see Fig. 6), whereas more magnesian rocks (Fig. 5) will experience mainly late growth of cordierite. Note that the more Fe-rich assemblages cross two andalusite-producing divariant fields. The second generation of andalusite shown in Fig. 8 is attributed to the second, higher-pressure divariant reaction.

field relationships at Petrel Cove imply that the Victor Harbor Granite was emplaced late in, or following, S2 development, we believe that the evidence for earlier magmatic activity both locally (Fig. 4a), as well as regionally (Foden *et al.*, 1999; Sandiford *et al.*, 1995), support the notion that the metamorphic heating is linked to the emplacement of granites nearby. The physical significance of the inferred increase in pressure, from <3 kbar to $>c.$ 4 kbar during S2 (and S3) development, while the rocks began to cool, is more contentious. Conventionally, the increase in pressure is associated with burial, and consequently we attribute it to the crustal thickening during the amplification of the D2 folds, which may well have been accompanied thrusting higher in the metamorphic pile.

DISCUSSION

The preceding discussion has detailed evidence for an 'anticlockwise' *P–T* evolution involving a pressure increase of *c.* 1 kbar during cooling and progressive deformation in the thermal aureole of the Victor Harbor Granite. Though numerous workers have documented essentially isobaric *P–T* paths associated heating and cooling at low pressures, evidence for pressure increase near peak temperatures is relatively rare, and the factors that might contribute to such paths have been poorly understood. Metamorphic *P–T* paths showing temperature excursions at low to moderate pressures are normally associated with magmatic heating (Lux *et al.*, 1986; Barton & Hanson, 1988; DeYoreo *et al.*, 1991; Collins & Vernon, 1991; Sandiford & Powell, 1991). As shown by Sandiford *et al.* (1991), the inverse exponential temperature dependence of lithospheric strength provides a logical reason for the coupling of deformation and heating that seems to be characteristic of such terranes (e.g. Vernon *et al.*, 1993; Karlstrom & Williams, 1995). In convergent settings, where deformation leads to crustal thickening, a thermo-mechanical coupling of this type should lead to 'anticlockwise' *P–T* paths as material points are buried tectonically during and following heating. Indeed, such 'anticlockwise' *P–T* evolutions should be the 'hallmark' of this thermo-mechanical coupling. Given the widespread occurrence of intermediate-temperature, low-pressure metamorphic terranes, we find it surprising that 'anticlockwise' *P–T* paths involving significant compression at elevated temperatures have not been documented from more localities. Whether this reflects a scarcity of terranes with such *P–T* histories, or a misinterpretation of the *P–T* records, remains to be seen.

The association of granite emplacement, deformation and metamorphism observed at Petrel Cove raises questions relating to the temporal and spatial distribution of deformation at the regional scale. Granites such as the Victor Harbor Granite and the Reedy Creek Granite have deformed thermal aureoles associated with regional D2 fabric development. At Reedy Creek, some 80 km NNE of Petrel Cove, the deformation apparently occurred within a few million years of 490 Ma (J. Foden, personal communication 2001). In contrast, the age of deformation at Victor Harbor is poorly constrained at older than 508 ± 14 Ma. This suggests that the S2 fabric may be regionally diachronous, with deformation in different parts of the orogen reflecting variations in the thermal state of the lithosphere due to the heterogeneous production and ascent of magmas through the lithosphere (Stuwe *et al.*, 1993). Since peak metamorphic temperatures are of the order of 550°–600 °C through the internal parts of this belt, this prospect may well be amenable to testing with detailed thermochronologic studies designed to elucidate the high temperature cooling history of the sequences.

One of the intriguing aspects of the structural-metamorphic evolution of the Petrel Cove Formation in the vicinity of the Victor Harbor Granite is the presence of a pre-S2 foliation that is preserved in the cordierite and andalusite porphyroblasts in the highest grade areas. This early foliation had a near-horizontal orientation (Steinhardt, 1989). In lower grade areas around 1 km to the west, there is no evidence of an early foliation, or structures that predate the regional upright NE-trending folds. A similar relationship occurs on a more regional scale elsewhere in the southern Adelaide Fold Belt where a recumbent fabric predates the regional upright fabric in the highest grade areas, whereas in adjacent lower grade regions there is no early recumbent fabric (Sandiford *et al.*, 1995; Oliver & Zakowski, 1995). At Petrel Cove, the spatial association between an extensive belt of granite that includes the Victor Harbor Granite as well as other older intrusives and metamorphism and deformation suggests the formation of multiple structural fabrics is directly linked to the presence of the granite. One possibility is that flow of material away from the belt of granite magmatism as melts ascended through the crust resulted in localised recumbent fabrics that are subsequently overgrown by peak metamorphic porphyroblasts as the region immediately surrounding the granite undergoes heating.

ACKNOWLEDGEMENTS

This research was supported by an ARC-large grant to M. Sandiford, an ARC postdoctoral fellow award to B. Worley and project DGYCIT PB94-0684-CO2-02 to G. Alias. We thank R. Offler, M. Rubenach, G. Clarke, P. James and R. Powell for their comments of an earlier draft of this manuscript.

REFERENCES

Adshead-Bell, N. S. & Bell, T. H., 1999. The progressive development of a macroscopic upright fold pair during five near orthogonal foliation producing events: complex

microstructures versus a simple macrostructure. *Tectonophysics*, **306,** 121–147.
Barton, M. D. & Hanson, R. B., 1988. Magmatism and the development of low pressure metamorphic belts: implications from the western United States and thermal modeling. *Bulletin of the Geological Society of America*, **101,** 1051–1065.
Chen, Y. D. & Liu, S. F., 1996. Precise U-Pb zircon dating of a post-D2 meta-dolerite: constraints for rapid tectonic development of the southern Adelaide Fold Belt during the Cambrian. *Journal of the Geological Society of London*, **153,** 83–90.
Collins, W. J. & Vernon, R. H., 1991. Orogeny associated with anticlockwise *P-T-t* paths: Evidence from low-P, high-T metamorphic terranes in the Arunta Inlier, central Australia. *Geology*, **19,** 835–838.
Cooper, J., Jenkins, R. J. F., Compston, W. & Williams, I. S., 1992. Ion-probe zircon dating of a mid-Early Cambrian tuff in South Australia. *Journal of the Geological Society of London*, **149,** 185–192.
Cull, J. P., 1982. An appraisal of Australian heat-flow data. *BMR Journal of Australian Geology and Geophysics*, **7,** 11–21.
Daily, B. & Milnes, A. R., 1973. Stratigraphy, structure and metamorphism of the Kanmantoo Group (Cambrian) in its type section east of Tunkalilla beach, South Australia. *Transactions of the Royal Society of South Australia*, **97,** 213–242.
Dasch, E. J., Milnes, A. R. & Nesbitt, R. W., 1971. Rubidium-strontium geochronology of the Encounter Bay Granite and adjacent metasedimentary rocks, South Australia, *Journal of the Geological Society of Australia*, **18,** 259–266.
DeYoreo, J. J., Lux, D. R. & Guidotti, C. V., 1991. Thermal modeling in low-pressure/high-temperature metamorphic belts. *Tectonophysics*, **188,** 209–238.
Dymoke, P. & Sandiford, M., 1992. Phase relations of Buchan facies series pelitic assemblages: calculations and application to the Mount Lofty Ranges, South Australia. *Contributions to Mineralogy and Petrology*, **110,** 121–132.
Flottmann, T., Gibson, G. & Kleinschmidt, G., 1993. Structural continuity of the Ross and Delamerian orogens of Antarctica and Australia along the margin of the paleo-Pacific. *Geology*, **21,** 319–322.
Foden, J., Sandiford, M., Dougherty-Page, J. & Willliams, I., 1999. Geochemistry and geochronology of the Rathjen Gneiss: implications for the early tectonic evolution of the Delamerian Orogen. *Australian Journal of Earth Science*, **46,** 377–389.
Holland, T. J. B. & Powell, R., 1990. An internally-consistent thermodynamic dataset with uncertainties and correlations: the system Na_2O-K_2O-CaO-MgO-FeO-Fe_2O_3-Al_2O_3-SiO_2-TiO_2-C-H_2-O_2. *Journal of Metamorphic Geology*, **8,** 89–124.
Jenkins, R. F. J. & Sandiford, M., 1992. Observations on the tectonic evolution of the southern Adelaide Fold Belt. *Tectonophysics*, **214,** 27–36.
Karlstrom, K. & Williams, M., 1995. The case for simultaneous deformation, metamorphism and plutonism: an example from Proterozoic rocks in central Arizona. *Journal of Structural Geology*, **17,** 59–81.
Liu, S. F. & Fleming, P. D., 1990. Mafic dykes and their tectonic setting in the southern Adelaide Foldbelt, South Australia. In: *Mafic Dykes and Emplacement Mechanism* (eds A. J. Parker, P. C. Rickwood & D. H. Tucker), pp. 401–413. Balkema, Rotterdam.
Lux, D. R., DeYoreo, J. J., Guidotti, C. V. & Decker, E. R., 1986. Role of plutonism in low-pressure metamorphic belt formation. *Nature*, **323,** 795–797.
Milnes, A. R., Compston, W. & Daily, B., 1977. Pre- to syntectonic emplacement of early Palaeozoic granites in south-eastern South Australia. *Journal of the Geological Society of Australia*, **24,** 87–106.
Offler, R. & Fleming, P. D., 1968. A synthesis of folding and metamorphism in the Mount Lofty Ranges, South Australia. *Journal of the Geology Society of Australia*, **15,** 245–266.
Oliver, N. H. S. & Zakowski, S., 1995. Timing and geometry of deformation, low-pressure metamorphism and anatexis in the eastern Mt. Lofty Ranges: the possible role of extension. *Australian Journal of Earth Sciences*, **42,** 501–507.
Pattison, D. R. M., 1987. Variations in Mg/(Mg + Fe), F, (Fe,Mg) Si-2Al in pelitic minerals in the Ballachulish thermal aureole, Scotland. *American Mineralogist*, **72,** 255–272.
Pattison, D. R. M., Spear, F. S. & Cheney, J. T., 1999. Polymetamorphic origin of muscovite + cordierite + staurolite + biotite assemblages: implications for the metapelitic petrogenetic grid and fro *P-T* paths. *Journal of Metamorphic Geology*, **17,** 685–703.
Powell, R. & Holland, T. J. B., 1988. An internally consistent thermodynamic data set with uncertainties and correlations: 3. Applications to geobarometry, worked samples and a computer program. *Journal of Metamorphic Geology*, **6,** 173–204.
Powell, R. & Holland, T. J. B., 1990. Calculated mineral equilibria in the pelite system KFMASH (K_2O-FeO-MgO-Al_2O_3-SiO_2-H_2O). *American Mineralogist*, **75,** 367–380.
Powell, R., Holland, T. J. B. & Worley, B., 1998. Calculating phase diagrams involving solid solutions via non-linear equations, with examples using THERMOCALC. *Journal of Metamorphic Geology*, **16,** 575–586.
Sandiford, M., Foden, J., Zhou, S. & Turner, S., 1992. Granite genesis and the mechanics on convergent orogenic belts with application to the southern Adelaide Fold Belt. *Proceedings of the Royal Society of Edinburgh (Hutton Symposium Volume)*, **83,** 83–93.
Sandiford, M., Fraser, G., Arnold, J., Foden, J. & Farrow, T., 1995. Some causes and consequences of High-T, Low-P metamorphism, Mount Lofty Ranges. *Australian Journal of Earth Sciences*, **42,** 233–240.
Sandiford, M. & Hand, M., 1998. Australian Proterozoic high-temperature metamorphism in the conductive limit. In: *What Controls Metamorphism, Special Publication 138* (eds Treloar, P. & O'Brien, P.), pp. 103–114. Geological Society, London.
Sandiford, M., Martin, N., Zhou, S. & Fraser, G., 1991. Mechanical consequences of granite emplacement during high-T, low-P metamorphism and the origin of 'anticlockwise' *P-T* paths. *Earth and Planetary Science Letters*, **107,** 164–172.
Sandiford, M. & Powell, R., 1991. Some remarks on high temperature-low pressure metamorphism in convergent orogens. *Journal of Metamorphic Geology*, **9,** 333–340.
Sleep, N. H., 1979. A thermal constraint on the duration of folding with reference to Acadian geology, New England (USA). *Journal of Geology*, **87,** 583–589.
Spear, F. S. & Cheney, J. T., 1989. A petrogenetic grid for pelitic schists in the system K_2O-FeO-MgO-Al_2O_3-SiO_2-H_2O. *Contributions to Mineralogy and Petrology*, **101,** 149–164.
Steinhardt, C., 1989. Lack of porphyroblast rotation in non-coaxially deformed schist from Petrel Cove, South Australia, and its implications. *Tectonophysics*, **158,** 127–140.
Stuwe, K., Sandiford, M. & Powell, R., 1993. Episodic metamorphism and deformation events in low pressure, high temperature terrains. *Geology*, **21,** 829–832.
Thompson, J. B., 1957. The graphical analysis of mineral assemblages in pelitic schists. *American Mineralogist*, **42,** 842–858.
Vernon, R. H., Collins, W. J. & Paterson, S. R., 1993. Pre-foliation metamorphism in low-pressure/high-temperature terrains. *Tectonophysics*, **219,** 241–256.
Xu, G., Will, T. M. & Powell, R., 1994. A calculated petrogenetic grid for rocks in the system K_2O-FeO-MgO-Al_2O_3-SiO_2-H_2O, with particular reference to contact metamorphosed pelites. *Journal of Metamorphic Geology*, **12,** 99–119.

Received 11 August 2000; revision accepted 10 September 2001.